Draft version August 14, 2018
Typeset using LaTeX **twocolumn** style in AASTeX61

RED AND REDDENED: ULTRAVIOLET THROUGH NEAR-INFRARED OBSERVATIONS OF TYPE Ia SUPERNOVA 2017erp*

Peter J. Brown,[1,2] Griffin Hosseinzadeh,[3,4] Saurabh W. Jha,[5] David Sand,[6] Ethan Vieira,[7] Xiaofeng Wang,[8] Mi Dai,[5] Kyle G. Dettman,[5,9] Syed Uddin,[10] Lifan Wang,[1,2,10] Iair Arcavi,[3,4,11,12] Tiara Diamond,[13,14] Daichi Hiramatsu,[3,4] D. Andrew Howell,[3,4] E. Y. Hsiao,[15] G. H. Marion,[16] Curtis McCully,[3,4] Peter A. Milne,[6] Davron Mirzaqulov,[14] Stefano Valenti,[17] and Danfeng Xiang[8]

[1] *Department of Physics and Astronomy, Texas A&M University, 4242 TAMU, College Station, TX 77843, USA*
[2] *George P. and Cynthia Woods Mitchell Institute for Fundamental Physics & Astronomy*
[3] *Las Cumbres Observatory, 6740 Cortona Dr. Suite 102, Goleta, CA, 93117-5575, USA*
[4] *University of California, Santa Barbara, Department of Physics, Santa Barbara, CA, 93106-9530, USA*
[5] *Department of Physics and Astronomy, Rutgers the State University of New Jersey, 136 Frelinghuysen Road, Piscataway, NJ 08854 USA*
[6] *Steward Observatory,University of Arizona, 933 North Cherry Avenue,Tucson, AZ 85721, USA*
[7] *Department of Aerospace Engineering, Texas A&M University, 4242 TAMU, College Station, TX 77843, USA*
[8] *Physics Department/Tsinghua Center for Astrophysics, Tsinghua University; Beijing, 100084, China*
[9] *Centre for Astrophysics and Supercomputing, Swinburne University of Technology, Melbourne, Victoria, Australia*
[10] *Purple Mountain Observatory, Chinese Academy of Sciences, Nanjing, Jiangshu, China*
[11] *Einstein Fellow*
[12] *The Raymond and Beverly Sackler School of Physics and Astronomy, Tel Aviv University, Tel Aviv 69978, Israel*
[13] *Goddard Space Flight Center, 8800 Greenbelt Rd, Greenbelt, MD 20771, USA*
[14] *Ulugh Beg Astronomical Institute, Uzbekistan Academy of Sciences, Uzbekistan, Tashkent, 100052, Uzbekistan*
[15] *Department of Physics, Florida State University, Tallahassee, FL 32306, USA*
[16] *University of Texas at Austin, 1 University Station C1400, Austin, TX, 78712-0259, USA*
[17] *Department of Physics, University of California, Davis, 1 Shields Avenue, Davis, CA 95616-5270, USA*

ABSTRACT

We present space-based ultraviolet/optical photometry and spectroscopy with the *Swift* Ultra-Violet/Optical Telescope and Hubble Space Telescope, respectively, along with ground-based optical photometry and spectroscopy and near-infrared spectroscopy of supernova SN 2017erp. The optical light curves and spectra are consistent with a normal Type Ia supernova (SN Ia). Compared to previous photometric samples in the near-ultraviolet (NUV), SN 2017erp has colors similar to the NUV-red category after correcting for Milky Way and host dust reddening. We find the difference between SN 2017erp and the NUV-blue SN 2011fe is not consistent with dust reddening alone but is similar to the SALT color law, derived from rest-frame UV photometry of higher redshift SNe Ia. This chromatic difference is dominated by the intrinsic differences in the UV and only a small contribution from the expected dust reddening. Differentiating the two can have important consequences for determining cosmological distances with rest-frame UV photometry. This spectroscopic series is important for analyzing SNe Ia with intrinsically redder NUV colors. We also show model comparisons suggesting that metallicity could be the physical difference between NUV-blue and NUV-red SNe Ia, with emission peaks from reverse fluorescence near 3000 Å implying a factor of ten higher metallicity in the upper layers of SN 2017erp compared to SN 2011fe. Metallicity estimates are very model dependent however, and there are multiple effects in the UV. Further models and UV spectra of SNe Ia are needed to explore the diversity of SNe Ia which show seemingly independent differences in the near-UV peaks and mid-UV flux levels.

Corresponding author: Peter J. Brown
pbrown@physics.tamu.edu

* Based on observations made with the NASA/ESA Hubble Space Telescope, obtained at the Space Telescope Science Institute, which is operated by the Association of Universities for Research in Astronomy, Inc., under NASA contract NAS 5-26555. These observations are associated with program #14665.

Keywords: supernovae: general — supernovae: individual (SN2017erp) — supernovae: individual (SN2011fe) — supernovae: individual (SN2011by) — supernovae: individual (SN2015F) — ultraviolet: general

1. INTRODUCTION

Type Ia supernovae (SNe Ia) are excellent standard candles because their optical absolute magnitudes have a low dispersion, which can be further reduced using relationships between the absolute magnitude of a SN and its light curve shape and/or colors (Phillips 1993; Riess et al. 1996; Phillips et al. 1999; Tripp & Branch 1999; Goldhaber et al. 2001; Wang et al. 2005). SNe Ia are used to constrain cosmological parameters such as Ω_M and Λ and the dark energy equation of state (e.g. Riess et al. 1998; Perlmutter et al. 1999; Riess et al. 2004; Betoule et al. 2014; Scolnic et al. 2018).

Despite this optical uniformity, SNe Ia have been found to be much more diverse at ultraviolet (UV) wavelengths (Ellis et al. 2008; Foley et al. 2008b; Brown et al. 2010; Cooke et al. 2011; Wang et al. 2012; Milne et al. 2013; Brown 2014; Brown et al. 2014b; Foley et al. 2016) with systematic differences between the SNe Ia observed in the rest-frame near-UV (NUV; covering roughly 2700-4000 Å) locally and at redshifts z>0.3 (Foley et al. 2012; Maguire et al. 2012; Milne et al. 2015).

One of the unexpected results from the large sample of *Swift* SNe is a possible bimodal distribution of the NUV-optical colors of optically "normal" SNe Ia. Milne et al. (2013) find about 1/3 of SNe Ia (dubbed "NUV-blue") to have significantly bluer (by about 0.5 mag) NUV to optical colors. The majority of nearby SNe Ia belong to the NUV-red category (though the fractions depend on whether and how extinction is corrected; Brown et al. 2017), so they might be considered the most "normal" SNe Ia. A well-studied example of a NUV-red SN Ia is the "golden standard" SN 2005cf (Wang et al. 2009a). SN 2011fe is now used as the de facto standard of normality, but it is actually among the bluest of the NUV-blue SNe (Brown et al. 2017).

UV spectroscopic comparisons have mostly focused on the NUV because of the steep drop in flux shortward of that and the limited wavelength range redshifted into the optical (Foley et al. 2008a; Ellis et al. 2008; Foley et al. 2008b; Bufano et al. 2009; Cooke et al. 2011; Wang et al. 2012; Maguire et al. 2012; Foley et al. 2016; Pan et al. 2018). UV photometric studies have found that the photometric scatter in peak luminosity increases at shorter wavelengths (Brown et al. 2010). The NUV-blue SNe are generally bluer than the NUV-red (or at least less catastrophically red) in the mid-UV (MUV; 1600 to 2500 Å), but there is a lot of scatter and some overlap. The differences are strongest at early times but seem to converge at a common color after about twenty days after maximum light. At early epochs the UV comes from the outermost layers of the SN ejecta, so this could probe either progenitor metallicity or the density gradient of the layers from which the UV is emitted. While the general increase in dispersion to shorter wavelengths could have a single cause, Foley & Kirshner (2013) identified two "twin" SNe Ia which have nearly identical spectra in the NUV and optical but different continuum levels in the MUV. This suggests the UV dispersion could have multiple components from different sources.

Many physical differences have strong effects in the UV (Brown et al. 2015), including metallicity (Höflich et al. 1998; Lentz et al. 2000; Sauer et al. 2008; Walker et al. 2012), asymmetry (Kasen & Plewa 2007; Kromer & Sim 2009), and density gradients (Sauer et al. 2008; Mazzali et al. 2014). Dust reddening is a strong external effect (e.g. Amanullah et al. 2014; Foley et al. 2014; Brown et al. 2015). Most of the modelling has been done with limited UV information, with SNe 2010gn and 2011fe well-studied exceptions (Hachinger et al. 2013; Mazzali et al. 2014).

Timmes et al. (2003) and Mazzali & Podsiadlowski (2006) showed how a change in the metallicity of the progenitor can affect the ratio of radioactive to non-radioactive Ni, and thus the luminosity and width of the light curve in a way not accounted for in the empirical relations (see also Miles et al. 2016). This could be the origin of the luminosity difference between the optical twins SNe 2011by and 2011fe (Foley & Kirshner 2013; Graham et al. 2015; Foley et al. 2018). Metallicity differences could be responsible for the scatter in the luminosity-width relations seen locally and lead to systematic differences at high redshift due to chemical evolution of the universe as a whole and the individual star formation history in the individual galaxies and star forming regions in which the progenitors are formed (Höflich et al. 2000; Podsiadlowski et al. 2006; Bravo et al. 2010; Moreno-Raya et al. 2016). Metallicity differences will appear strongest in the UV due to the larger line opacities (cf. Lentz et al. 2000; Sauer et al. 2008; Walker et al. 2012). However, the other physical differences mentioned above (e.g. density gradients, asymmetry, explosion models) have strong effects in the UV (Brown et al. 2015, 2018). Determining whether the UV dispersion is caused by something like metallicity, which evolves with redshift, or asymmetry/viewing angle, which does not, is important to the cosmological impact of the UV dispersion.

Despite the NUV-red SNe Ia being the majority of local SNe Ia (Milne et al. 2015), the three most normal SNe Ia with high signal-to-noise (S/N) UV spectroscopy from the Hubble Space Telescope (*HST*) are all NUV-blue SNe Ia, including the twin NUV-blue

SNe 2011by and 2011fe (Foley & Kirshner 2013), and SN 2015F (Foley et al. 2016), which appears to be a reddened NUV-blue SN Ia. The existing NUV spectra of NUV-red SNe Ia do not have coverage below 2500 Å to see how the flux differences extend into the mid-UV. Such spectra are also necessary for understanding the extinction and k-corrections and the effect of "red-leak" optical contamination in the *Swift*/UVOT filters. This motivated an *HST* program (#14665; PI: Brown) "Ultraviolet Spectra of a Normal Standard Candle." In this paper we present the first *HST* UV spectroscopy of a normal, albeit reddened, NUV-red SN Ia. The *HST*, *Swift*, and ground-based observations are described in Section 2. The observations are analyzed in Section 3, with physical interpretation and consequences discussed in Section 4. We summarize in Section 5.

2. OBSERVATIONS

2.1. *Discovery and Host Galaxy*

SN 2017erp was discovered by Itagaki (2017) in images taken on 2017-06-13 15:01:28. It was classified by Jha et al. (2017) as an extremely young SN Ia.

The host galaxy of SN 2017erp is NGC 5861, classified as SAB(rs)c (de Vaucouleurs et al. 1991), at a redshift of 0.006174 ± 0.000003 (Theureau et al. 2005). The redshift corresponds to a distance modulus of 32.30 ± 0.26 assuming a Hubble constant of 73 km s^{-1} Mpc^{-1} and a random velocity uncertainty of 300 km s^{-1}. Observations with the Hubble Space Telescope have already been made for the purpose of determining a more accurate distance to the host galaxy using Cepheid variables (PI: Riess).

2.2. *Swift Photometry*

Swift began observing SN 2017erp on 2017-06-14 04:55:33 UT with six photometric filters: uvw2, uvm2, uvw1, u, b, and v. Filter details are available in Roming et al. (2005); Breeveld et al. (2011). The photometry was reduced using the pipeline of the *Swift* Optical/Ultraviolet Supernova Archive (SOUSA; Brown et al. 2014a). The light curves are shown in Figure 1. The extremely red early colors prompted us to trigger our *HST* program once we confirmed that they were not solely due to dust reddening. This assessment was done using color evolution and color-color evolution plots of young SNe Ia previously observed with *Swift*/UVOT as well as the UV/optical spectral template of SN 2011fe (Pereira et al. 2013) with different amounts of reddening applied to map out the parameter space covered by a reddened NUV-blue SN Ia (Brown et al. 2017).

2.3. *HST/STIS Spectroscopy*

Observations with the *HST* were triggered as part of the program "Ultraviolet Spectra of a Normal Standard Candle" to obtain UV spectroscopy. Four epochs were obtained with the *HST*'s Space Telescope Imaging Spectrograph (STIS) using the G430L grism and the CCD detector and the G230L grism and the MAMA detector. For these spectra we use the default *HST* reduction obtained from the Mikulski Archive for Space Telescopes (MAST[1]). We eliminate bad pixels and cosmic rays, smooth the spectra in 5 Å bins, and combine the MUV G230L and NUV/optical G430L spectra. The four epochs are displayed in Figure 2.

2.4. *Ground-based Optical Photometry*

Optical light curves and spectra come from the Global Supernova Project, a three-year Key Project to observe lightcurves and spectroscopy of hundreds of SNe using the Las Cumbres Observatory global network of 21 robotic telescopes. *UBVgri* images were taken with the Sinistro cameras on the Las Cumbres Observatory network of 1-meter telescopes (Brown et al. 2013). Point-spread-function (PSF) photometry was extracted using `lcogtsnpipe` (Valenti et al. 2016), a PyRAF-based photometric reduction pipeline. *UBV* Vega magnitudes are calibrated to Landolt standard fields taken at the same site and on the same night as observations of the SN. *gri* AB magnitudes are calibrated to the Sloan Digital Sky Survey.

Broadband BVRI-band photometric observations of SN 2017erp were also obtained with the Tsinghua-NAOC 0.8-m telescope (TNT) at Xinglong Observatory in China (Huang et al. 2012) and AZT-22 1.5 m telescope (hereafter AZT) at Madanak Astronomical Observatory in Uzbekistan, spanning the phases from +2 to +28 days relative to the B-band maximum light. All CCD images were pre-processed using standard routines, which includes corrections for bias, flat field, and removal of cosmic rays. As the SN is located relatively far from the galactic center, we did not apply a techinique of subtracting the galaxy template from the SN images; instead, the foreground sky was determined locally and subtracted. The instrumental magnitudes of both the SN and the reference stars were then measured using the standard point spread function (PSF). These magnitudes are converted to those of the standard Johnson system using the APASS catalogue[2].

[1] https://archive.stsci.edu/hst/
[2] https://www.aavso.org/apass

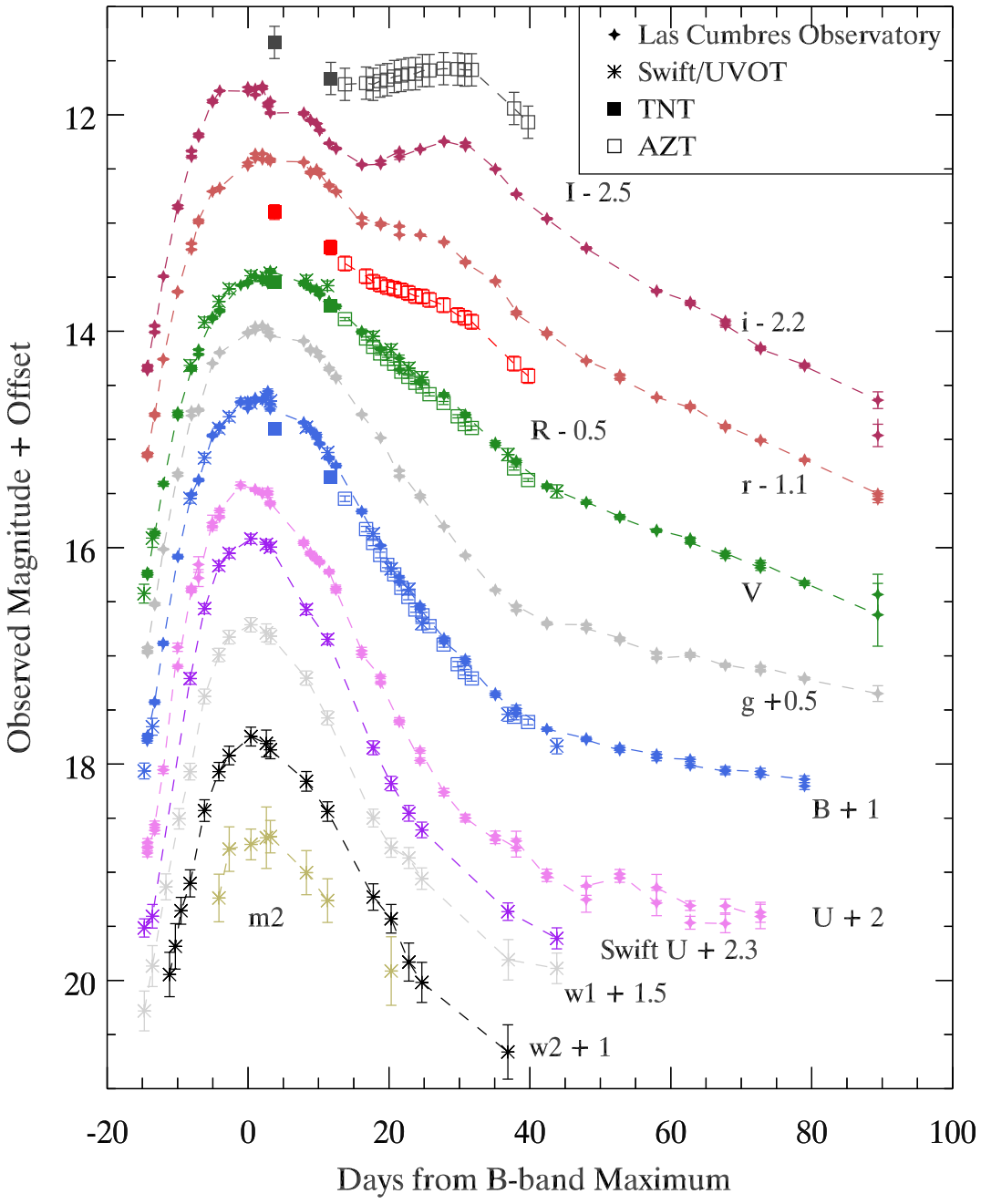

Figure 1. Photometry of SN 2017erp from the Swift/UVOT, the Las Cumbres Observatory network, Xinglong Observatory, and Madanak Astronomical Observatory.

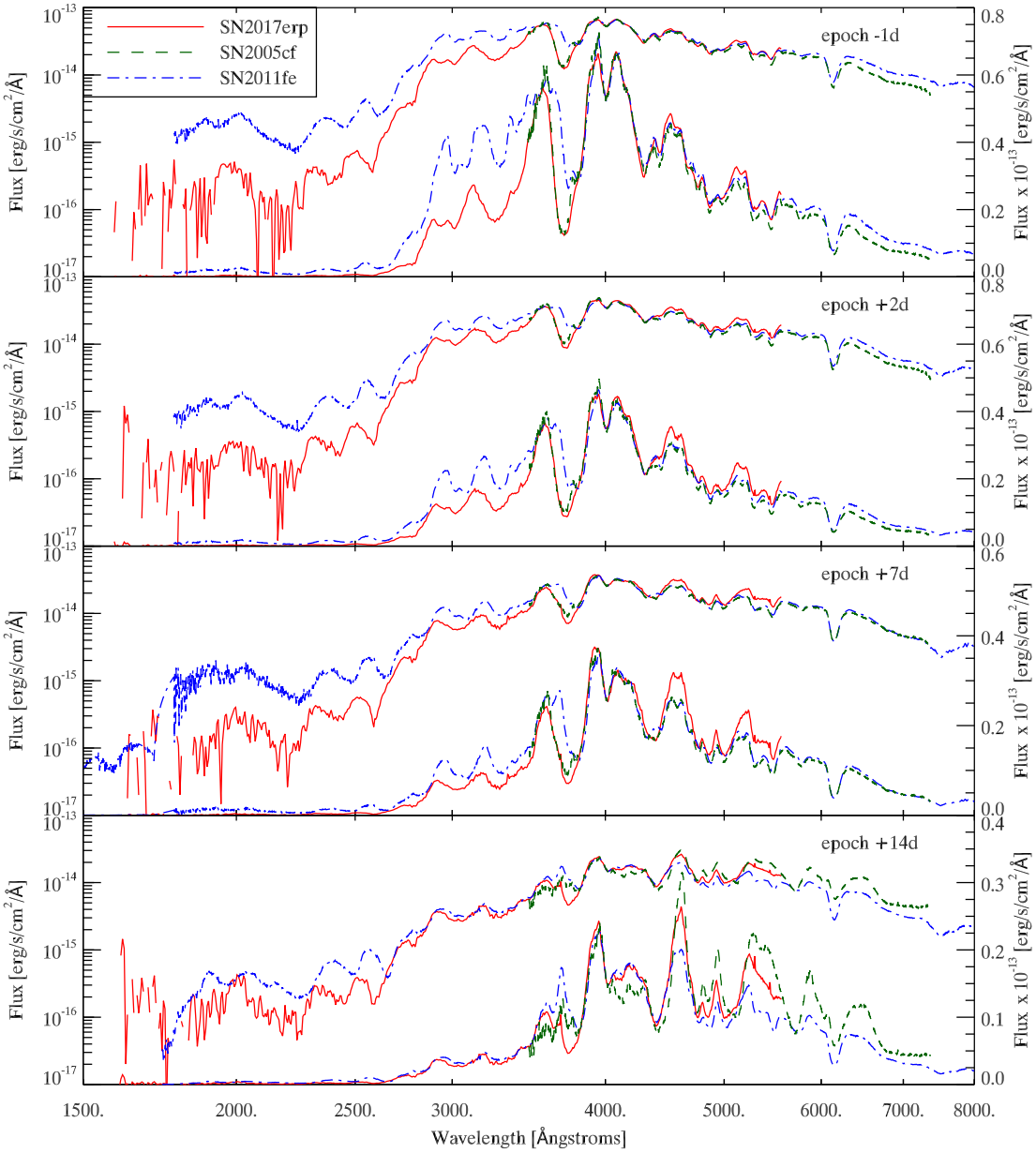

Figure 2. The four epochs of SN 2017erp UV spectroscopic observations (combined with optical spectra from nearby epochs and corrected for MW and host reddening) are compared with SNe 2005cf and 2011fe. The observed flux is displayed in logarithmic (top curves in each panel with units on the left y-axis) and linear (lower curves with units on the right) scales, with the spectra of the comparison SNe scaled to match SN 2017erp around 4000 Å.

2.5. *Optical Spectroscopy*

Spectra were taken with the robotic FLOYDS spectrographs on Las Cumbres Observatory's 2-meter telescopes on Haleakalā, Hawai'i, and in Siding Spring, Australia, and were reduced using the PyRAF-based `floydsspec` pipeline. Additional spectra were taken with the Southern African Large Telescope (SALT) using the Robert Stobie Spectrograph (Smith et al. 2006) as part of program 2017-1-MLT-002 (PI: Jha). We used the PG0900 grating and 1.5″ longslit, yielding a spectral resolution $\lambda/\Delta\lambda \approx 900$ over the wavelength range 3500–9400 Å. The data were reduced with a custom pipeline that incorporates routines from PyRAF and PySALT[3] (Crawford et al. 2010). A series of spectra of SN 2017erp also were obtained with the Xinglong 2.16-m telescope (XLT+BFOSC) of NAOC, China, the 2.3-m Australian National University (ANU) telescope (+WiFeS), and the 6.5-m Magellan telescope (+IMACS). All of the spectra were mangled to match the *BVgri* photometry at that epoch, except for the first SALT spectrum which predated the photometry. The optical spectra are displayed in Figure 3, and the observation dates and wavelength ranges of all the spectra are given in Table 1.

2.6. *Gemini NIR Spectroscopy*

One epoch of NIR spectroscopy was obtained with the FLAMINGOS-2 (Eikenberry et al. 2008) spectrograph at Gemini South. The FLAMINGOS-2 data were taken with the JH grism and filter in place, along with a 0.72 arcsec slit width, yielding a wavelength range of 1.0 - 1.8 μm and R$\sim$1000. The FLAMINGOS-2 longslit data were reduced in a standard way (i.e. image detrending, sky subtraction of the AB pairs, spectral extraction, spectral combination and wavelength calibration) using the F2 pyraf package provided by Gemini Observatory. An A0V star was observed near in time and position to the science data in order to make a telluric absorption correction and to flux calibrate the spectra, following the methodology of Vacca et al. (2003). This spectrum is combined with an *HST* UV spectrum and a smoothed Las Cumbres Observatory optical spectrum in Figure 4.

3. ANALYSIS

3.1. *Light Curve Parameters and the Reddening*

We used the SuperNovae in object-oriented Python (SNooPy; Burns et al. 2011) light curve fitter on the Las Cumbres Observatory BVgri photometry to determine various light curve parameters. The B band reached a maximum brightness of 13.27 ± 0.01 mag on MJD 57934.9 (UT 2017-06-30.9). The Δm_{15}, a parameterization of the templates and not filter specific, is measured to be 1.05 ± 0.06 and the color stretch (Burns et al. 2014) s_{BV}=0.993 ± 0.03. Thus SN 2017erp has a very standard light curve shape.

[3] http://pysalt.salt.ac.za/

3.2. *Reddening and the Intrinsic Color of SN 2017erp*

The line of sight dust extinction through the Milky Way (MW) is estimated to be A_V=0.296 based on the Schlegel et al. (1998) dust maps recalibrated by Schlafly & Finkbeiner (2011), corresponding to E($B-V$)=0.095 mag assuming R_V=3.1. As an estimate of the total reddening, we compare the B_{peak}-V_{peak} pseudocolor to Equation 7 of Phillips et al. (1999), yielding a total E($B-V$) of 0.23 mag. An alternative estimate of the reddening comes by comparing $B-V$ colors between 30 and 90 days after the time of V-band maximum to the Lira relation (Phillips et al. 1999). The total E($B-V$) color excess has an average of 0.29 mag and a standard deviation of 0.03 mag compared to the Lira relation. The "color stretch" version of the Lira law gives a total E($B-V$)=0.41 ± 0.03 mag (Burns et al. 2014).

Light curve fitters such as SALT2 (Guy et al. 2010), MLCS2k2 (Jha et al. 2007), and SNooPy (Burns et al. 2011) use more of the light curve in determining the color differences, and thus reddening, between the SN Ia being fit and the training sample. The optical light curves are fit with the SALT2 model (Guy et al. 2010) using the SNCosmo package (Barbary et al. 2016). The best fit parameters are: $m_B = 13.28$, $x_1 = 0.46$ and $c = 0.05$, where m_B is the peak magnitude at rest frame B band, x_1 is the shape parameter and c is the color parameter. Using the Tripp relation (Tripp 1998): $\mu = m_B + \alpha x_1 - \beta c - M$ and setting $\alpha = 0.14$, $\beta = 3.1$, and $M = -19.1$, we determine the distance modulus as 32.29 ± 0.12, where the uncertainty has been estimated based on the typical scatter for SN Ia. The MLCS2k2 (Jha et al. 2007) fit to the optical light curve data with Milky Way E(B-V) = 0.095 yields $\Delta = -0.21 \pm 0.02$ and host $A_V = 0.55 + / - 0.04$ for fixed host $R_V = 1.9$. This corresponds to a host E(B-V) = 0.29 +/- 0.02 and thus a total $E(B-V) = 0.38$. The MLCS2k2 distance modulus is 32.07 ± 0.09 (on an H_0 = 72 km/s/Mpc scale) favoring more extinction and a closer distance modulus than the SALT2 model and the Hubble flow distance modulus of 32.30 mag. The color model of SNooPy estimates the E($B-V$)$_{host}$=0.179 ± 0.005 (statistical) ± 0.060 (systematic) mag with R_V=2.80 ± 0.51. Fitting similar to Prieto et al. (2006) yields E($B-V$)$_{host}$=0.097 ± 0.005 (statistical) ± 0.060 (systematic) mag, assuming R_V=3.1.

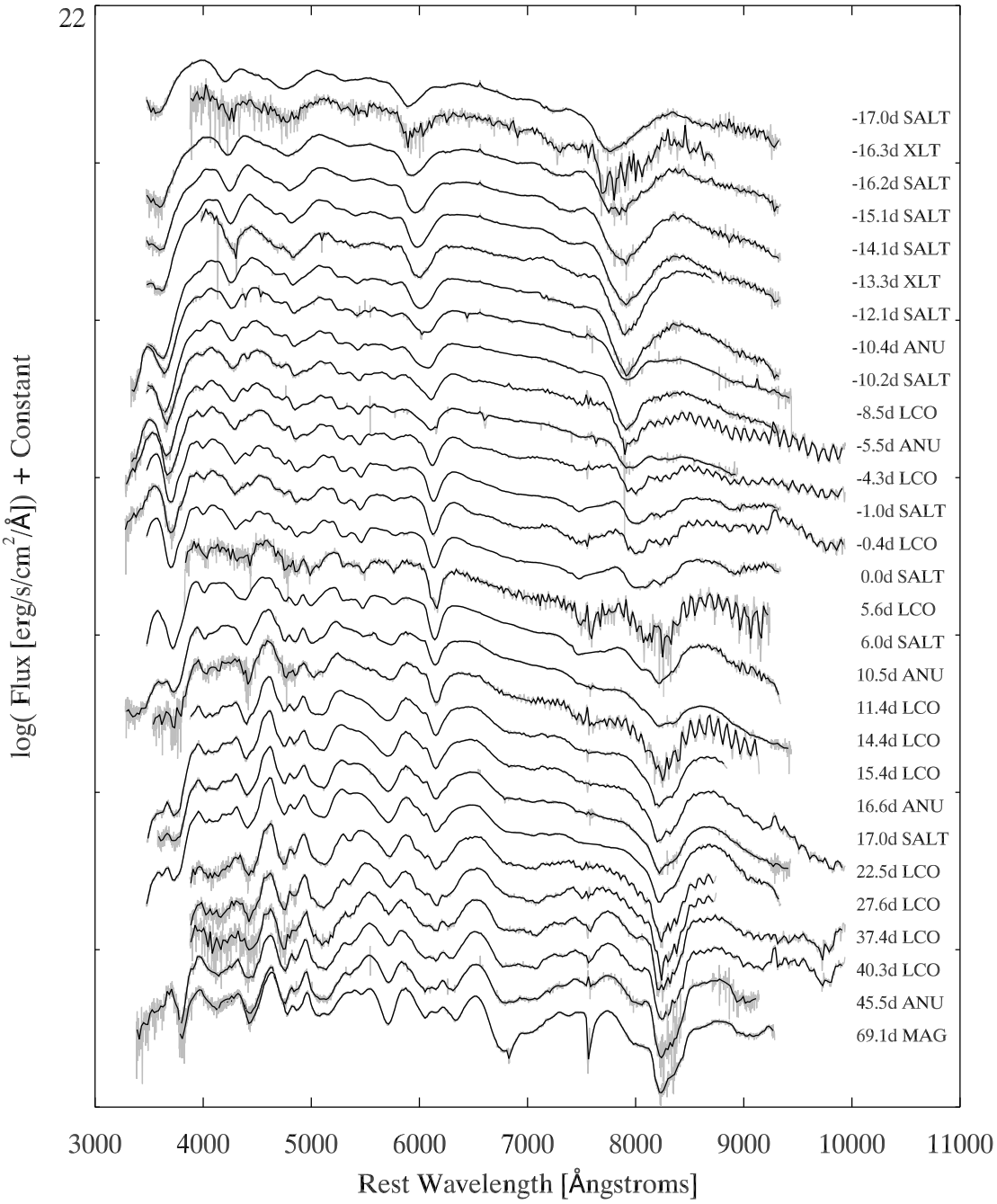

Figure 3. Optical spectral series of SN 2017erp presented in the rest frame of SN 2017erp. Original spectra (with some regions of low S/N trimmed out) are plotted in grey. A smoothed version of the spectra (10 Å bins) is plotted in black. Except for the first spectrum, all have been modified (i.e. warped or mangled) using a low-order polynomial to match the photometry.

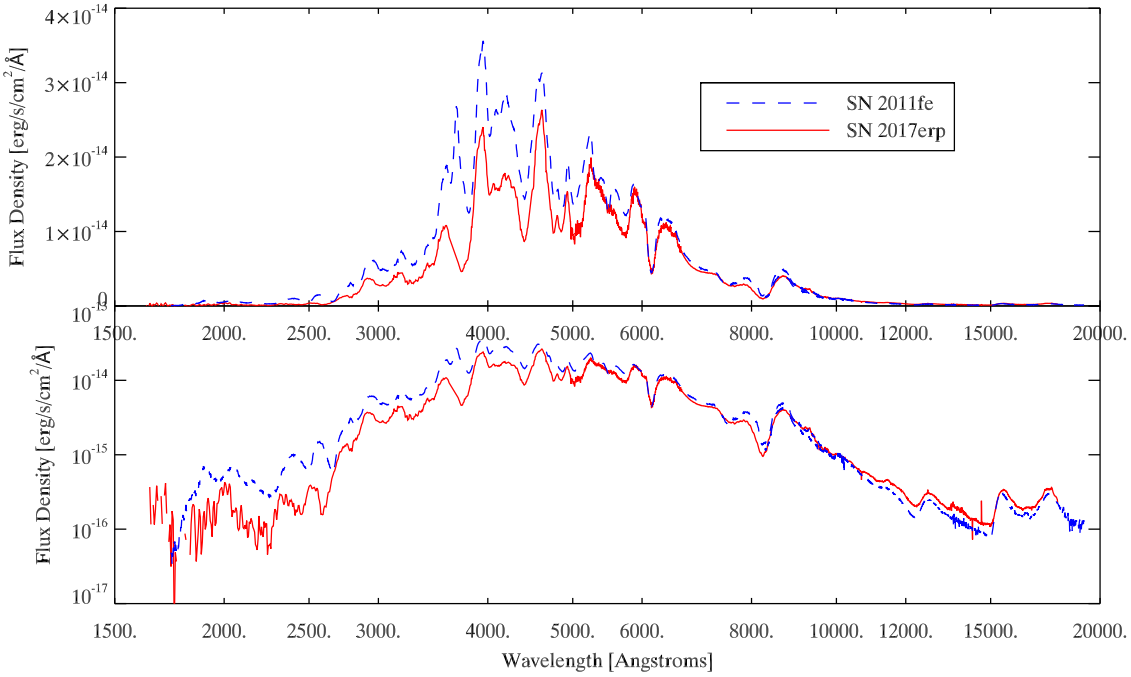

Figure 4. Combined and extinction-corrected UV/optical/NIR spectra of SNe 2017erp (10 days after B-band maximum) and 2011fe (9 days after B-band maximum; Mazzali et al. 2014) are compared. SN 2017erp has been reddening corrected based on the MW dust extinction from Schlafly & Finkbeiner (2011) and the host color excess from SNooPy.

We use this latter, smaller estimate of E($B-V$)=0.097 mag for the host reddening as the larger values result in extreme blue peak optical colors ($B-V$=-0.29 mag for MLCS2k2) which do not match other SNe Ia. The optical spectra show absorption by interstellar Na I D from both the Milky Way and the host galaxy NGC 5861 with comparable strengths, consistent with this smaller value of E($B-V$) for the host galaxy. However, quantifying extinction from low-resolution spectra is notoriously unreliable (Phillips et al. 2013). The absolute magnitudes resulting from different reddening values could be used as a further constraint, but we postpone such a discussion until a better distance measurement is available.

The color evolution and peak maximum light colors of SN 2017erp are consistent with the NUV-red SNe Ia as defined by Milne et al. (2013). However, as shown in Brown et al. (2017), some SNe Ia with observed colors similar to NUV-red SNe could be NUV-blue SNe reddened by dust. Determining the intrinsic colors is complicated by the possibility of different intrinsic optical colors (Milne et al. 2013), uncertainty in the appropriate dust reddening law, and how much the intrinsic spectral differences would affect the broad-band filter extinction coefficients determined from a NUV-blue spectral template like SN 2011fe. The latter uncertainty is removed by having a new spectral sequence of a NUV-red SN Ia. In Figure 5 we show the peak color of SN 2017erp with those of the Brown et al. (2017) sample with $1.0 < \Delta M_{15}(B) < 1.4$. Lines show the reddening vectors for SN 2011fe and SN 2017erp corresponding to different dust reddening laws. The dust reddening laws include the Cardelli et al. (1989) law parameterized with R_V=3.1 (like the MW) and R_V=1.7 (similar to that found for SNe Ia; e.g., Kessler et al. 2009), an extinction law measured for the SMC (Prevot et al. 1984), and a Large Magellenic Cloud extinction law modified by circumstellar scattering (Goobar 2008; Brown et al. 2010). We also show symbols corresponding to dereddening the SN 2017erp spectrum for MW reddening with E($B-V$)=0.095 mag and R_V=3.1 and after correcting for the MW reddening and the SNooPy estimated host reddening of E($B-V$)=0.097 mag (with R_V=3.1).

The dereddened colors of SN 2017erp are about 0.5 mag redder in the uvw1-v color than the low reddened SN 2011fe, with comparable colors to several NUV-red SNe Ia. This makes the SN 2017erp *HST* spectral series complementary to those of the NUV-blue SNe 2011fe (Mazzali et al. 2014) and 2011by (Foley & Kirshner 2013) and the reddened NUV-blue SN 2015F[4] (Foley et al. 2016). A diversity in spectral templates to match the observations is important regardless of whether the SNe Ia at the NUV-blue and NUV-red ends represent distinct groups or a continuously varying color difference.

3.3. *Spectroscopic Comparisons*

3.3.1. *Optical Spectra*

The full optical spectral evolution of SN 2017erp is shown in Figure 3. The velocity of the Si II 6355 Å absorption begins at a high velocity of 21.5 Mm s^{-1} (Jha et al. 2017) but drops quickly to a value of 10.4 Mm s^{-1} at maximum light. The early velocity is actually that of a high-velocity component. The asymmetric Si II profile eleven days before maximum light shows the transition between the feature being dominated by the high velocity component to being dominated by the photospheric component. SN 2009ig showed similar behavior, and Marion et al. (2013) measured the velocity evolution of the separate components. Figure 6 shows the velocity evolution of the Si II 6355 line (considering only the dominant component) and demonstrates SN 2017erp is not significantly different than the "gold standards" SNe 2011fe (Pereira et al. 2013; Zhang et al. 2016) and 2005cf (Pastorello et al. 2007; Garavini et al. 2007; Wang et al. 2009a) in terms of photospheric velocity evolution. At shorter wavelengths, the Ca II H&K feature also begins by being very broad and stretched to blue wavelengths. By day 15 (though probably earlier where our spectra are noisier) the Ca II H&K feature is split into two distinct features with a high velocity feature at a similar velocity as near maximum light. A more detailed examination of the optical spectroscopic parameters is beyond the scope of this paper.

Milne et al. (2013) found that SNe Ia with high-velocities (HV; Si II ejecta velocities greater than about 12 Mm s^{-1} Wang et al. 2009b) are almost exclusively NUV-red, while normal-velocity SNe Ia can be either NUV-red or NUV-blue. Brown et al. (2018) confirmed this, showing that SNe Ia with normal velocities have a range of UV colors with no correlation with the velocities. Thus the photospheric velocity does not differentiate NUV-red and NUV-blue SNe Ia, consistent with the optical similarities seen here. However, the similarity in the high-velocity features of SNe 2017erp and 2005cf suggest a possibility that high velocity features may be related to the similar NUV-red colors. This would be consistent with the high velocity features and the UV

[4] SN 2015F being a reddened NUV-blue is also consistent with the detection of C II in optical spectra (Cartier et al. 2017).

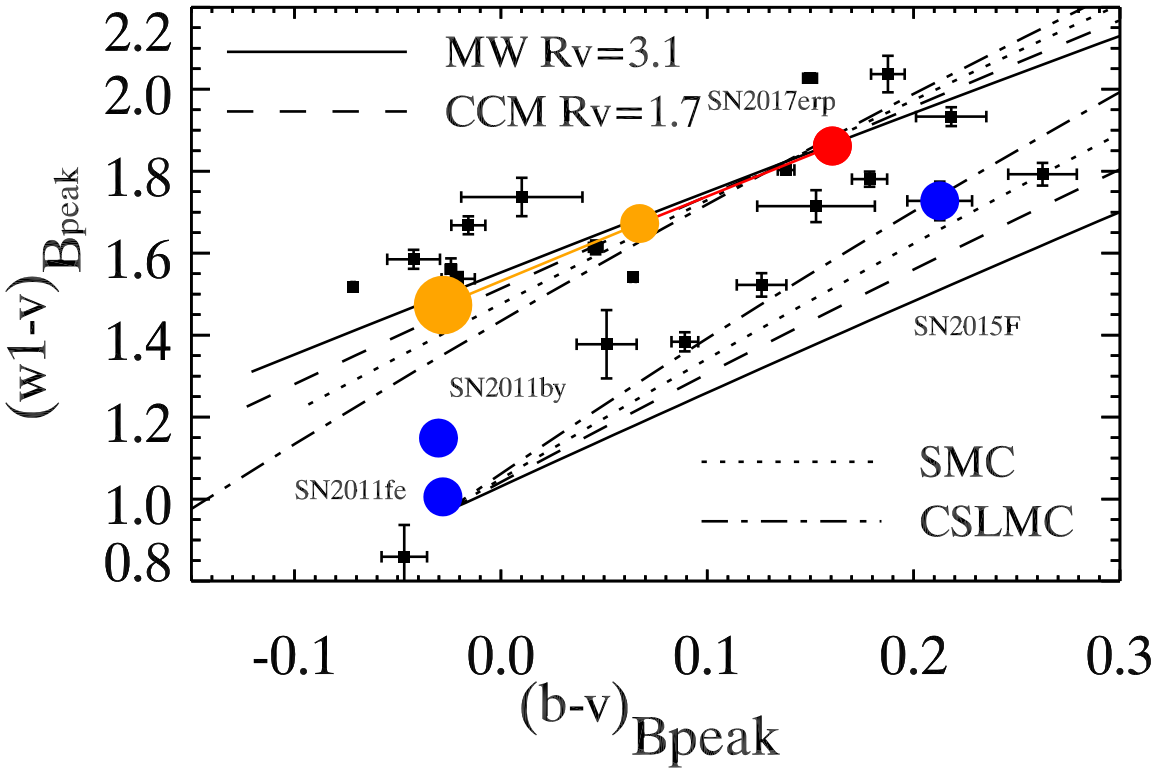

Figure 5. Colors of normal SNe Ia observed with *Swift*. SNe Ia observed with *HST* are plotted with solid circles, with SN 2017erp in red and the others in blue. Lines show the color-color vectors of SN 2011fe reddened and SN 2017erp reddened and unreddened with various reddening laws to show which of the observed SNe could have similar intrinsic colors and only differ by being more or less reddened. SN 2017erp is shown dereddened by the MW extinction and the SNooPy-inferred host reddening as progressively larger orange circles. The vertical spread in $uvw1-v$ for objects with similar $B-V$ color is evidence for intrinsic color scatter not related to dust reddening.

continuum both arising from the outer layers of the SN ejecta.

3.3.2. *Near-infrared Spectrum*

Figure 4 compares SN 2017erp at 10.2 days after maximum light from ∼1600–18000 Å with SN 2011fe at a comparable epoch. The SN 2011fe spectrum is a combination of an *HST* UV spectrum from Mazzali et al. (2014) and a Gemini GNIRS near-infrared spectrum from Hsiao et al. (2013). At wavelengths longer than 5000 Å, SNe 2017erp and 2011fe are nearly identical.

The Gemini spectrum of SN 2017erp was conveniently taken near the epoch when the H-band break near 1.5 microns is strongest. Dividing the peak flux on the long side of the break by the minimum flux on the short wavelength side, we calculate the H-band break ratio R_{12}=3.0 ± 0.1. This is lower than SN 2011fe, but consistent with SN 2005cf (see Figure 11 in Hsiao et al. 2013). This fits in the correlation between H-band break ratio and light curve parameter found by Hsiao et al. (2013, 2015).

3.3.3. *Ultraviolet Spectra*

Having established SN 2017erp as having colors similar to the NUV-red SNe Ia, we wish to compare directly the UV spectroscopic properties between the NUV-red and NUV-blue groups with these high-quality *HST* spectra. Previous comparisons in these regions have used lower S/N spectra from UVOT, *HST*'s ACS grism, and ground-based optical spectra of higher redshift SNe Ia (Ellis et al. 2008; Foley et al. 2008b; Cooke et al. 2011; Maguire et al. 2012; Wang et al. 2012; Milne et al. 2013, 2015; Smitka 2016). *HST* spectra in the near-UV covered this region for a sample of SNe Ia (Cooke et al. 2011; Maguire et al. 2012). As shown in Figure 2, the spectral shapes and features near maximum light of SNe 2017erp, 2011fe, and 2005cf are nearly identical longward of 4000 Å. SNe 2005cf and 2017erp continue to be similar in the Ca H&K feature (which is not solely Ca H&K, see e.g. Foley 2013) with a single absorption deeper and bluer than the double feature seen in SN 2011fe. Blueward of that the continuum of SN 2017erp is depressed relative to that of SN 2011fe and instead of two strong peaks as in SN 2011fe, the bluer of the two is basically absent in SN 2017erp. These fea-

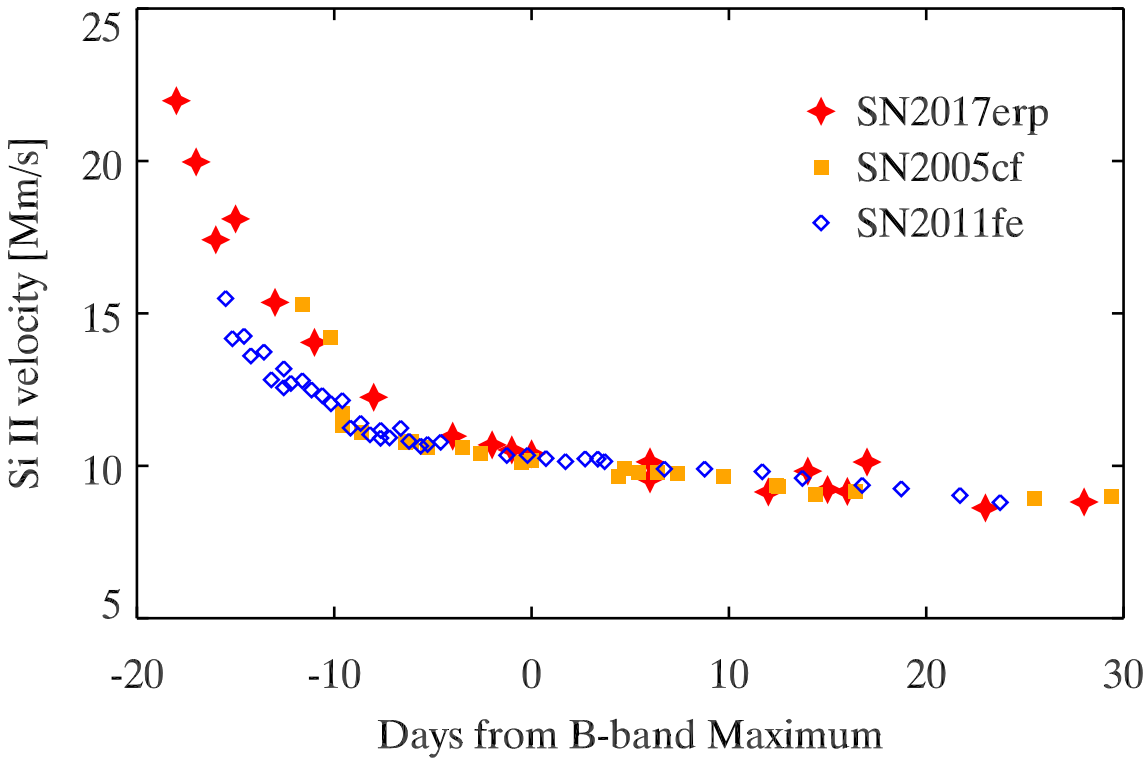

Figure 6. The photospheric velocity of SN 2017erp is compared to SNe 2005cf and 2011fe, showing a similar behavior and value near maximum light.

tures are identified as λ_1 and λ_2 in Ellis et al. (2008) and Maguire et al. (2012). The features appear shifted to the blue in SN 2017erp similar to an increase in velocity despite the similar photospheric velocities near maximum light. As explained in Walker et al. (2012), large metallicities will increase the opacity, causing the UV features to appear at even higher velocities (the UV normally forms at higher velocity layers the optical lines). This is consistent with the near-UV dispersion existing for SNe Ia with small and similar photospheric velocities (Brown et al. 2018). This also makes metallicity, ejecta density gradients, and ejecta velocities linked to each other rather than separate parameters that can be easily distinguished.

The overall flux difference between SNe 2011fe and 2017erp increases at shorter wavelengths into the mid-UV. These are the first spectra revealing the mid-UV properties of a NUV-red SN Ia.

4. DISCUSSION

4.1. *Interpreting Intrinsic Differences as Reddening*

Now we examine how the intrinsic differences seen here could be interpreted as peculiar dust extinction. In Figure 7 we compare the difference between SNe 2017erp and 2011fe to the various reddening laws discussed previously and the color law used in the SALT2 light curve fitter (Guy et al. 2010; Betoule et al. 2014). Because we are interested in the shape of the wavelength dependence, the laws have been scaled to give the same $B-V$ differences as between the SNe and then shifted to zero in the V band. The difference between SNe 2011fe and 2017erp matches broadly the shape of the SALT2 color law (which itself is made from a polynomial fit to broad-band observations of higher redshift SNe Ia between 2800 - 7000 Å and extrapolated to wavelengths above and below that; Guy et al. 2010).

We suggest that in the UV, the steep intrinsic differences could dominate the derivation and use of the SALT2 color law over dust reddening. The SALT2 color law is derived empirically and combines the potential effects of dust reddening and intrinsic color variations. This is difficult to disentangle in the optical, where both dust reddening and intrinsic red color seem to correlate with lower luminosity (e.g., Scolnic et al. 2014). However, the NUV differences do not appear to correlate with luminosity (Maguire et al. 2012; Brown et al. 2017). The use of UV colors to correct for reddening could lead to biased distances especially if the UV colors may change with redshift (Milne et al. 2015; but see also Cinabro et al. 2017).

We have focused on the colors and relative flux levels, as a well-measured distance to the host of SN 2017erp is

not yet available. NGC 5861 has been observed earlier this year by the *HST* in order to measure the periods of Cepheid variables (PI: Riess) and calculate a distant in a consistent manner with SNe 2011by, 2011fe and others (Riess et al. 2016; Foley et al. 2018). This will also shed light on the differences in dust extinction and inferred distance modulus estimated for SN 2017erp by the different light curve fitters.

4.2. *Metallicity as a Possible Origin for the Near-ultraviolet Differences*

Understanding the origin of the UV differences is important to better characterizing the progenitors and explosion mechanisms of SNe Ia and how they might change with redshift. Following comparisons from Smitka (2016) that the NUV-blue/red spectral difference between 2700 and 3300 Å (see also Milne et al. 2013, 2015) could be caused by metallicity, we next compare the Walker et al. (2012) models to SNe 2011fe and 2017erp. We use a maximum light spectrum of SN 2011fe from Mazzali et al. (2014) and our maximum light spectrum of SN 2017erp dereddened by a MW extinction law with R_V=3.1 and E($B-V$)=0.18 mag.

We find a reasonable match between SN 2011fe and the model with one-fifth the metallicity, while SN 2017erp matches the model with a factor of two increase in metallicity. These comparisons are shown in Figure 8. The main features are those identified as λ_1 and λ_2 in Ellis et al. (2008) and found by Walker et al. (2012) to be caused by reverse flourescence. This is consistent with the range found by Smitka (2016) using *Swift*/UVOT grism spectra for the NUV-red sample. If the NUV differences are solely due to metallicity and the magnitude of the Walker et al. (2012) models is correct, that would imply a factor of ten difference in the metallicity between SNe 2011fe and 2017erp. It is important to note that Walker et al. (2012) explicitly note that their method of altering the model metallicity cannot distinguish between primordial metallicity of the progenitor and upmixing of products of explosive nucleosynthesis. Continuing blueward, the mid-UV flux of SN 2017erp falls well below that of SN 2011fe and the best-fitting Walker et al. (2012) model. Foley & Kirshner (2013) have demonstrated using SNe 2011by and 2011fe that SNe with nearly identical optical and near-UV spectra can have very different continuum levels in the mid-UV. Thus a separate mechanism must affect the mid-UV independent from the near-UV. The Walker et al. (2012) models were not first principle models, nor based on either of these objects, but abundances and density gradients were adjusted to match UV/optical spectra of SN 2005cf near maximum light. Other differences in the spectra are thus not accounted for, but we seek general trends causing the largest differences between SNe 2011fe and 2017erp. Similar to Foley & Kirshner (2013) we have compared two well-observed examples, but larger samples (Smitka 2016; Pan et al. 2018) of SNe Ia might help disentangle multiple effects.

There is a connection between our proposed cause of the NUV-blue/red dispersion and the general trend seen by Thomas et al. (2011) and Milne et al. (2013) that the NUV-blue SNe Ia frequently have detections of CII in their spectra while NUV-red SNe Ia generally do not (with SN 2005cf a notable exception; Silverman et al. 2012). Heringer et al. (2017) found that emission from iron can hide the absorption from carbon, implying that SNe Ia with carbon signatures have a lower metal content in their outer layers. SN 2017erp would be another exception to this general trend, as there are dips in the early optical spectra redward of Si II 6355 Å which may be CII. However the presence of CII and its detectability is not a binary property, and Parrent et al. (2011) discussed a variety of causes (such as S/N, abundance, and velocity differences) which may affect if and at what epochs CII is detectable. If metallicity is related to both the NUV dispersion and the strength of CII features, all would be expected to have a continuous distribution. A larger sample of SNe Ia with measurements of UV color and the strengths of CII (corrected to some common epoch) is needed to understand this further.

Foley & Kirshner (2013) and Graham et al. (2015) conjecture that metallicity is the cause of the mid-UV flux differences of the otherwise nearly identical SNe 2011fe and 2011by based on comparisons with models from Lentz et al. (2000). Since multiple models show near-UV differences (Höflich et al. 1998; Sauer et al. 2008; Walker et al. 2012; Wang et al. 2012; Baron et al. 2015; Miles et al. 2016) including the near-peak and later models of Lentz et al. (2000), we are confident that at least some of the differences in the near-UV are caused by metallicity. The differences between the models, however, and the other factors affecting the UV make us cautious about quantitative statements regarding metallicity using the models. Further work is needed to resolve to what extent the differences between SNe 2011fe and 2011by and between SNe 2011fe and 2017erp are due to metallicity and how much is due to other causes. What we do think is clear, however, is that there are multiple regimes of UV dispersion – SNe Ia with similar optical colors and light curve shapes can have different near-UV colors and spectra (Milne et al. 2013; Brown et al. 2017), and SNe Ia with similar optical and near-UV colors and light curve shapes can

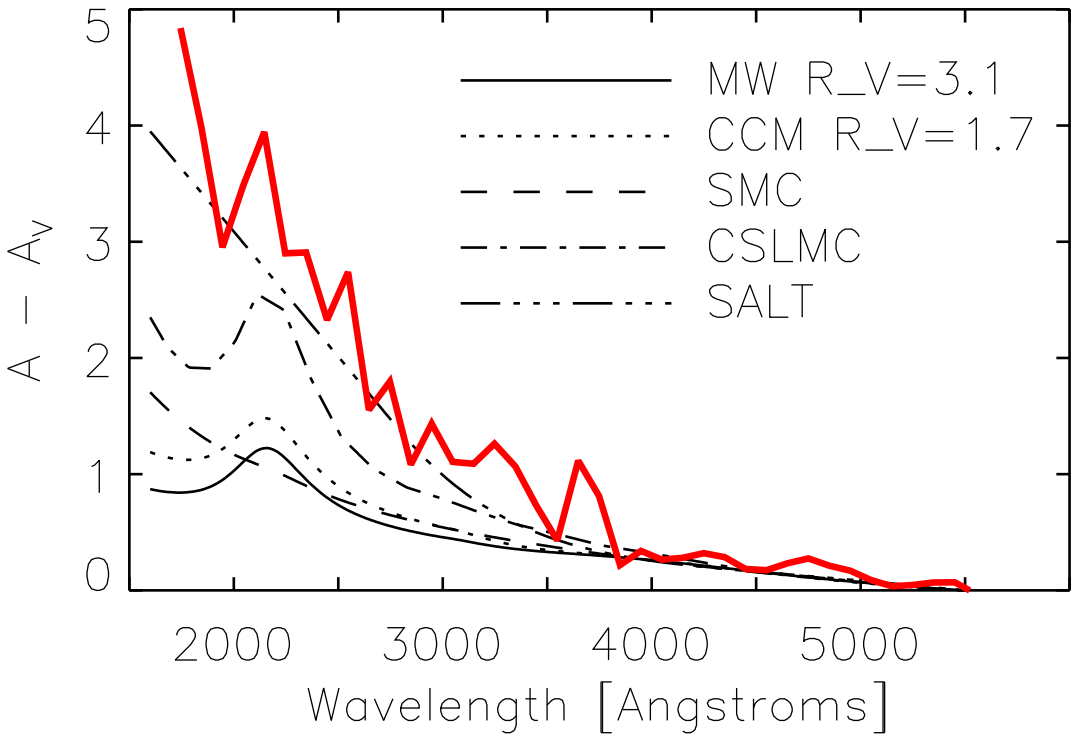

Figure 7. The difference between the spectra of SNe 2011fe and 2017erp in magnitudes is compared to various reddening laws normalized to have the same $B-V$ effect and all shifted to zero in the V band.

have different mid-UV flux (Foley & Kirshner 2013; Graham et al. 2015).

Foley et al. (2018) further tie the metallicity differences they infer between SNe 2011fe and 2011by to the significant luminosity differences between them without affecting the optical colors or spectra. Recent modeling by Miles et al. (2016) predicts that a change in progenitor metallicity does cause a change in the bolometric luminosity in the same direction as predicted by Timmes et al. (2003) and assumed by Foley et al. (2018). The models also, however, predict a change in the ΔM_{15}(B) of up to 0.4 mag, depending on the model, and changes in the temperature and thus spectral shape as well as numerous features in the UV and the optical. This makes it difficult to isolate an effect like metallicity.

In scientific experiments, one changes a single physical characteristic at a time (the independent variable) and measure the difference (if any) on one or more other characteristics (dependent variables). In an observational science, we have a multitude of observables that may or may not be dependent on each other. We may attempt to limit the number of differences by using subsamples where one observable is similar. In this case we compare SNe Ia with similar velocities and ΔM_{15}(B) and seek the cause of a difference in the UV flux continuum and features. However, if the cause of the UV flux differences also causes differences in other observables such as velocity or ΔM_{15}(B), than such sample cuts may hide the relevant correlations.

The multiplicity of models predicting different UV effects from metallicity (Höflich et al. 1998; Lentz et al. 2000; Sauer et al. 2008; Walker et al. 2012; Miles et al. 2016) as well as the other effects which could be going on (asymmetry, density gradients, etc, see e.g. Brown et al. 2014b) make it seem premature to conclude metallicity is the cause of either the near-UV or mid-UV differences at this time. Multiple physical differences likely exist between SNe 2011fe and 2017erp which are not matched by the change of a single parameter like metallicity. What is needed are models which accurately predict the observed UV-optical-NIR spectra and light curves for a subset of SNe and grids of parameter variations. The large sample of UV, optical, and NIR spectra which now exist should be able to constrain the physical parameters that serve as inputs to the models.

5. SUMMARY

We have presented the first *HST* UV spectra of a normal, NUV-red SN Ia. We find differences in the near-UV associated with the Ca H&K feature and the continuum near 2800-3300 Å. The latter feature might be associ-

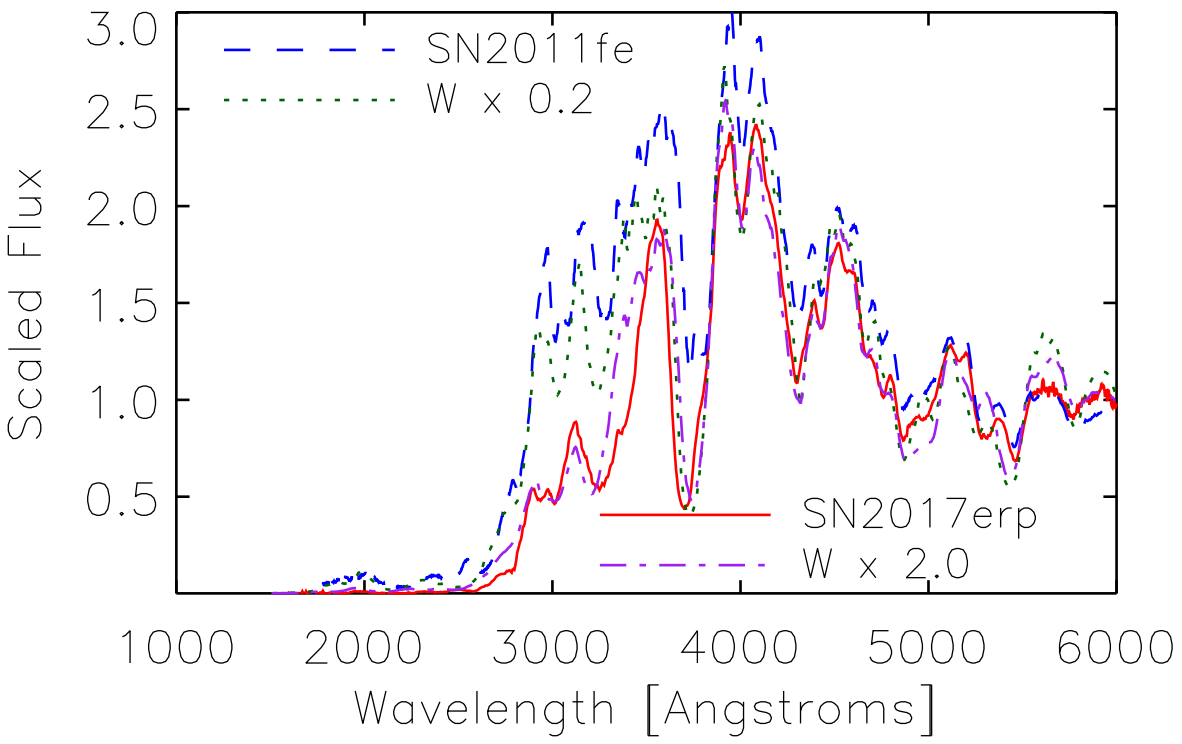

Figure 8. Maximum-light spectra of SNe 2011fe and 2017erp compared to models by Walker et al. (2012) with varying metallicity. SN 2011fe is similar in the near-UV to the model with 0.2 times the metallicity of the baseline model created for SN 2005cf. SN 2017erp is most similar to the model with 2 times the metallicity. Both of the models shown have the broad Ca H&K feature to match SN 2005cf.

ated with higher metallicity, but further modelling work is necessary to allow the disentangling of likely multiple effects. The spectral differences are consistent with the SALT color law, implying that the law could be dominated by intrinsic differences, not dust, in the UV. Understanding the UV better is important for using SNe Ia as standard candles in the distant universe where the UV is redshifted into the observed bands and evolution in the progenitor properties might result in differences in the observables used for cosmology.

We thank N. Suntzeff and K. Krisciunas for helpful comments and support during the process of analysis and writing. We acknowledge the work of Jeremy Mould, Ashley J. Ruiter, Joao Bento, Jamison Burke, Shuhrat A. Ehgamberdiev, Han Lin, Jun Mo, Liming Rui, and Lingzhi Wang in obtaining some of this data. Support for program #14665 was provided by NASA through a grant from the Space Telescope Science Institute, which is operated by the Association of Universities for Research in Astronomy, Inc., under NASA contract NAS 5-26555. The *Swift* Optical/Ultraviolet Supernova Archive (SOUSA) is supported by NASA's Astrophysics Data Analysis Program through grant NNX13AF35G. This work made use of public data in the *Swift* data archive and the NASA/IPAC Extragalactic Database (NED), which is operated by the Jet Propulsion Laboratory, California Institute of Technology, under contract with NASA. This work makes use of observations from the Las Cumbres Observatory network and the Global Supernova Project. DAH, CM, and GH are supported by NSF grant AST 1313484. Research by DJS is supported by NSF grants AST-1821967, 1821987, 1813708 and 1813466. Based on observations obtained at the Gemini Observatory under programs GS-2017A-Q-33 (PI: Sand). Gemini is operated by the Association of Universities for Research in Astronomy, Inc., under a cooperative agreement with the NSF on behalf of the Gemini partnership: the NSF (United States), the National Research Council (Canada), CONICYT (Chile), Ministerio de Ciencia, Tecnología e Innovación Productiva (Argentina), and Ministério da Ciência, Tecnologia e Inovação (Brazil). The data were processed using the Gemini IRAF package. We thank the queue service observers and technical support staff at Gemini Observatory for their assistance. Support for IA was provided by NASA through the Einstein Fellowship Program, grant PF6-170148. Some of the obser-

vations reported in this paper were obtained with the Southern African Large Telescope (SALT). This supernova research at Rutgers University is supported by NASA grant NNG17PX03C and US Department of Energy award DE-SC0011636. AJR has been supported by the Australian Research Council through grant numbers CE110001020 and FT170100243. Syed A Uddin was supported by the Chinese Academy of Sciences President's International Fellowship Initiative Grant No. 2016PM014.

Facilities: HST(STIS), Swift(UVOT), Las Cumbres Observatory, Gemini South (GMOS, Flamingos-2), SALT (RSS)

Software: IRAF, PyRAF, PySALT

REFERENCES

Amanullah, R., Goobar, A., Johansson, J., et al. 2014, ApJL, 788, L21

Barbary, K., Barclay, T., Biswas, R., et al. 2016, SNCosmo: Python library for supernova cosmology, Astrophysics Source Code Library, , , ascl:1611.017

Baron, E., Hoeflich, P., Friesen, B., et al. 2015, MNRAS, 454, 2549

Betoule, M., Kessler, R., Guy, J., et al. 2014, A&A, 568, A22

Bravo, E., Domínguez, I., Badenes, C., Piersanti, L., & Straniero, O. 2010, ApJL, 711, L66

Breeveld, A. A., Landsman, W., Holland, S. T., et al. 2011, in American Institute of Physics Conference Series, Vol. 1358, GAMMA RAY BURSTS 2010. AIP Conference Proceedings, ed. J. E. McEnery, J. L. Racusin, & N. Gehrels, 373–376

Brown, P. J. 2014, ApJL, 796, L18

Brown, P. J., Baron, E., Milne, P., Roming, P. W. A., & Wang, L. 2015, ApJ, 809, 37

Brown, P. J., Breeveld, A. A., Holland, S., Kuin, P., & Pritchard, T. 2014a, A&SS, 354, 89

Brown, P. J., Landez, N. J., Milne, P. A., & Stritzinger, M. D. 2017, ApJ, 836, 232

Brown, P. J., Perry, J. M., Beeny, B. A., Milne, P. A., & Wang, X. 2018, ArXiv e-prints, arXiv:1807.10391

Brown, P. J., Roming, P. W. A., Milne, P., et al. 2010, ApJ, 721, 1608

Brown, P. J., Kuin, P., Scalzo, R., et al. 2014b, ApJ, 787, 29

Brown, T. M., Baliber, N., Bianco, F. B., et al. 2013, PASP, 125, 1031

Bufano, F., Immler, S., Turatto, M., et al. 2009, ApJ, 700, 1456

Burns, C. R., Stritzinger, M., Phillips, M. M., et al. 2011, AJ, 141, 19

—. 2014, ApJ, 789, 32

Cardelli, J. A., Clayton, G. C., & Mathis, J. S. 1989, ApJ, 345, 245

Cartier, R., Sullivan, M., Firth, R. E., et al. 2017, MNRAS, 464, 4476

Cinabro, D., Scolnic, D., Kessler, R., Li, A., & Miller, J. 2017, MNRAS, 466, 884

Cooke, J., Ellis, R. S., Sullivan, M., et al. 2011, ApJL, 727, L35

Crawford, S. M., Still, M., Schellart, P., et al. 2010, in Society of Photo-Optical Instrumentation Engineers (SPIE) Conference Series, Vol. 7737, Society of Photo-Optical Instrumentation Engineers (SPIE) Conference Series, 25

de Vaucouleurs, G., de Vaucouleurs, A., Corwin, Jr., H. G., et al. 1991, Third Reference Catalogue of Bright Galaxies. Volume I: Explanations and references. Volume II: Data for galaxies between 0^h and 12^h. Volume III: Data for galaxies between 12^h and 24^h.

Eikenberry, S., Elston, R., Raines, S. N., et al. 2008, in Society of Photo-Optical Instrumentation Engineers (SPIE) Conference Series, Vol. 7014, Society of Photo-Optical Instrumentation Engineers (SPIE) Conference Series, 0

Ellis, R. S., Sullivan, M., Nugent, P. E., et al. 2008, ApJ, 674, 51

Foley, R. J. 2013, MNRAS, 435, 273

Foley, R. J., Filippenko, A. V., & Jha, S. W. 2008a, ApJ, 686, 117

Foley, R. J., Hoffmann, S. L., Macri, L. M., et al. 2018, ArXiv e-prints, arXiv:1806.08359

Foley, R. J., & Kirshner, R. P. 2013, ApJL, 769, L1

Foley, R. J., Filippenko, A. V., Aguilera, C., et al. 2008b, ApJ, 684, 68

Foley, R. J., Filippenko, A. V., Kessler, R., et al. 2012, AJ, 143, 113

Foley, R. J., Fox, O. D., McCully, C., et al. 2014, MNRAS, 443, 2887

Foley, R. J., Pan, Y.-C., Brown, P., et al. 2016, MNRAS, 461, 1308

Garavini, G., Nobili, S., Taubenberger, S., et al. 2007, A&A, 471, 527

Goldhaber, G., Groom, D. E., Kim, A., et al. 2001, ApJ, 558, 359

Goobar, A. 2008, ApJL, 686, L103
Graham, M. L., Valenti, S., Fulton, B. J., et al. 2015, ApJ, 801, 136
Guy, J., Sullivan, M., Conley, A., et al. 2010, A&A, 523, A7
Hachinger, S., Mazzali, P. A., Sullivan, M., et al. 2013, MNRAS, 429, 2228
Heringer, E., van Kerkwijk, M. H., Sim, S. A., & Kerzendorf, W. E. 2017, ApJ, 846, 15
Höflich, P., Nomoto, K., Umeda, H., & Wheeler, J. C. 2000, ApJ, 528, 590
Höflich, P., Wheeler, J. C., & Thielemann, F. K. 1998, ApJ, 495, 617
Hsiao, E. Y., Marion, G. H., Phillips, M. M., et al. 2013, ApJ, 766, 72
Hsiao, E. Y., Burns, C. R., Contreras, C., et al. 2015, A&A, 578, A9
Huang, F., Li, J.-Z., Wang, X.-F., et al. 2012, Research in Astronomy and Astrophysics, 12, 1585
Itagaki, K. 2017, Transient Name Server Discovery Report, 647
Jha, S., Riess, A. G., & Kirshner, R. P. 2007, ApJ, 659, 122
Jha, S. W., Camacho, Y., Dettman, K., et al. 2017, The Astronomer's Telegram, 10490
Kasen, D., & Plewa, T. 2007, ApJ, 662, 459
Kessler, R., Becker, A. C., Cinabro, D., et al. 2009, ApJs, 185, 32
Kromer, M., & Sim, S. A. 2009, MNRAS, 398, 1809
Lentz, E. J., Baron, E., Branch, D., Hauschildt, P. H., & Nugent, P. E. 2000, ApJ, 530, 966
Maguire, K., Sullivan, M., Ellis, R. S., et al. 2012, MNRAS, 426, 2359
Marion, G. H., Vinko, J., Wheeler, J. C., et al. 2013, ApJ, 777, 40
Mazzali, P. A., & Podsiadlowski, P. 2006, MNRAS, 369, L19
Mazzali, P. A., Sullivan, M., Hachinger, S., et al. 2014, MNRAS, 439, 1959
Miles, B. J., van Rossum, D. R., Townsley, D. M., et al. 2016, ApJ, 824, 59
Milne, P. A., Brown, P. J., Roming, P. W. A., Bufano, F., & Gehrels, N. 2013, ApJ, 779, 23
Milne, P. A., Foley, R. J., Brown, P. J., & Narayan, G. 2015, ApJ, 803, 20
Moreno-Raya, M. E., Mollá, M., López-Sánchez, Á. R., et al. 2016, ApJL, 818, L19
Pan, Y.-C., Foley, R. J., Filippenko, A. V., & Kuin, N. P. M. 2018, MNRAS, 479, 517
Parrent, J. T., Thomas, R. C., Fesen, R. A., et al. 2011, ApJ, 732, 30
Pastorello, A., Taubenberger, S., Elias-Rosa, N., et al. 2007, MNRAS, 376, 1301
Pereira, R., Thomas, R. C., Aldering, G., et al. 2013, A&A, 554, A27
Perlmutter, S., Aldering, G., Goldhaber, G., et al. 1999, ApJ, 517, 565
Phillips, M. M. 1993, ApJL, 413, L105
Phillips, M. M., Lira, P., Suntzeff, N. B., et al. 1999, AJ, 118, 1766
Phillips, M. M., Simon, J. D., Morrell, N., et al. 2013, ApJ, 779, 38
Podsiadlowski, P., Mazzali, P. A., Lesaffre, P., Wolf, C., & Forster, F. 2006, ArXiv Astrophysics e-prints, arXiv:astro-ph/0608324
Prevot, M. L., Lequeux, J., Prevot, L., Maurice, E., & Rocca-Volmerange, B. 1984, A&A, 132, 389
Prieto, J. L., Rest, A., & Suntzeff, N. B. 2006, ApJ, 647, 501
Riess, A. G., Press, W. H., & Kirshner, R. P. 1996, ApJ, 473, 88
Riess, A. G., Filippenko, A. V., Challis, P., et al. 1998, AJ, 116, 1009
Riess, A. G., Strolger, L.-G., Tonry, J., et al. 2004, ApJ, 607, 665
Riess, A. G., Macri, L. M., Hoffmann, S. L., et al. 2016, ApJ, 826, 56
Roming, P. W. A., Kennedy, T. E., Mason, K. O., et al. 2005, Space Science Reviews, 120, 95
Sauer, D. N., Mazzali, P. A., Blondin, S., et al. 2008, MNRAS, 391, 1605
Schlafly, E. F., & Finkbeiner, D. P. 2011, ApJ, 737, 103
Schlegel, D. J., Finkbeiner, D. P., & Davis, M. 1998, ApJ, 500, 525
Scolnic, D. M., Riess, A. G., Foley, R. J., et al. 2014, ApJ, 780, 37
Scolnic, D. M., Jones, D. O., Rest, A., et al. 2018, ApJ, 859, 101
Silverman, J. M., Kong, J. J., & Filippenko, A. V. 2012, MNRAS, 425, 1819
Smith, M. P., Nordsieck, K. H., Burgh, E. B., et al. 2006, in Proc. SPIE, Vol. 6269, Society of Photo-Optical Instrumentation Engineers (SPIE) Conference Series, 62692A
Smitka, M. T. 2016, PhD thesis, Texas A&M University
Theureau, G., Coudreau, N., Hallet, N., et al. 2005, A&A, 430, 373
Thomas, R. C., Aldering, G., Antilogus, P., et al. 2011, ApJ, 743, 27
Timmes, F. X., Brown, E. F., & Truran, J. W. 2003, ApJL, 590, L83

Tripp, R. 1998, A&A, 331, 815

Tripp, R., & Branch, D. 1999, ApJ, 525, 209

Vacca, W. D., Cushing, M. C., & Rayner, J. T. 2003, PASP, 115, 389

Valenti, S., Howell, D. A., Stritzinger, M. D., et al. 2016, MNRAS, 459, 3939

Walker, E. S., Hachinger, S., Mazzali, P. A., et al. 2012, MNRAS, 427, 103

Wang, X., Wang, L., Zhou, X., Lou, Y.-Q., & Li, Z. 2005, ApJL, 620, L87

Wang, X., Li, W., Filippenko, A. V., et al. 2009a, ApJ, 697, 380

Wang, X., Filippenko, A. V., Ganeshalingam, M., et al. 2009b, ApJL, 699, L139

Wang, X., Wang, L., Filippenko, A. V., et al. 2012, ApJ, 749, 126

Zhang, K., Wang, X., Zhang, J., et al. 2016, ApJ, 820, 67

Table 1. Spectroscopic Observations of SN 2017erp

Epoch (days)	UT Time (yyyy-mm-dd hh:mm:ss)	Instrument	λ Start (Å)	λ End (Å)
-17.0	2017-06-13 22:14:34	SALT/RSS	3497	9400
-16.3	2017-06-14 14:45:03	XLT/BFOSC	3902	8790
-16.2	2017-06-14 17:55:06	SALT/RSS	3495	9398
-15.1	2017-06-15 18:08:17	SALT/RSS	3493	9397
-14.1	2017-06-16 18:03:51	SALT/RSS	3496	9397
-13.3	2017-06-17 14:49:53	XLT/BFOSC	4001	8779
-12.1	2017-06-18 18:04:46	SALT/RSS	3497	9398
-10.4	2017-06-20 12:54:50	ANU/WiFeS	3351	9500
-10.2	2017-06-20 17:52:04	SALT/RSS	3495	9397
-8.5	2017-06-22 09:29:26	LCO/Floyds	3501	10000
-5.5	2017-06-25 08:31:00	ANU/WiFeS	3351	9001
-4.3	2017-06-26 13:57:44	LCO/Floyds	3300	10000
-1.5	2017-06-29 10:24:23	HST/STIS/CCD	3000	5600
-1.4	2017-06-29 12:33:45	HST/STIS/MAMA	1585	3135
-1.0	2017-06-29 21:51:55	SALT/RSS	3497	9400
-0.4	2017-06-30 11:54:32	LCO/Floyds	3299	10000
0.0	2017-06-30 21:44:16	SALT/RSS	3496	9400
1.6	2017-07-02 11:26:15	HST/STIS/CCD	3000	5600
1.6	2017-07-02 11:26:15	HST/STIS/MAMA	1585	3135
5.6	2017-07-06 11:56:05	LCO/Floyds	3851	9298
6.0	2017-07-06 20:50:57	SALT/RSS	3499	9399
6.3	2017-07-07 05:43:08	HST/STIS/CCD	3000	5600
6.4	2017-07-07 07:41:15	HST/STIS/MAMA	1585	3135
10.2	2017-07-11 02:26:15	Gemini-South/FLAMINGOS-2	9860	18000
10.5	2017-07-11 09:45:07	ANU/WiFeS	3300	9499
11.2	2017-07-12 01:41:15	HST/STIS/CCD	3000	5600
11.3	2017-07-12 05:15:00	HST/STIS/MAMA	1585	3135
11.4	2017-07-12 08:16:09	LCO/Floyds	3551	9200
14.4	2017-07-15 07:12:04	LCO/Floyds	3901	8898
15.4	2017-07-16 06:51:48	LCO/Floyds	3500	10000
16.6	2017-07-17 10:51:17	ANU/WiFeS	3601	9489
17.0	2017-07-17 20:36:51	SALT/RSS	3497	9400
22.5	2017-07-23 08:37:29	LCO/Floyds	3901	8799
27.6	2017-07-28 11:03:13	LCO/Floyds	3901	8800
37.4	2017-08-07 06:30:13	LCO/Floyds	3902	10001
40.3	2017-08-10 05:51:04	LCO/Floyds	3402	10000
45.5	2017-08-15 08:35:38	ANU/WiFeS	3801	9198
69.1	2017-09-08 00:10:38	Magellan/IMACS	4161	9343